ENVIRONMENTAL STUDIES

How green can Amazon hydropower be? Net carbon emission from the largest hydropower plant in Amazonia

Dailson J. Bertassoli Jr.[1]*†, Henrique O. Sawakuchi[2], Kleiton R. de Araújo[3], Marcelo G. P. de Camargo[1], Victor A. T. Alem[1], Tatiana S. Pereira[3], Alex V. Krusche[4], David Bastviken[2], Jeffrey E. Richey[4,5], André O. Sawakuchi[1]

The current resurgence of hydropower expansion toward tropical areas has been largely based on run-of-the-river (ROR) dams, which are claimed to have lower environmental impacts due to their smaller reservoirs. The Belo Monte dam was built in Eastern Amazonia and holds the largest installed capacity among ROR power plants worldwide. Here, we show that postdamming greenhouse gas (GHG) emissions in the Belo Monte area are up to three times higher than preimpoundment fluxes and equivalent to about 15 to 55 kg CO_2eq MWh^{-1}. Since per-area emissions in Amazonian reservoirs are significantly higher than global averages, reducing flooded areas and prioritizing the power density of hydropower plants seem to effectively reduce their carbon footprints. Nevertheless, total GHG emissions are substantial even from this leading-edge ROR power plant. This argues in favor of avoiding hydropower expansion in Amazonia regardless of the reservoir type.

INTRODUCTION

The rise in energy demand on a global scale has increased the number of hydropower projects in tropical rivers. This trend raised attention on the negative outcomes of damming large rivers of the Amazon River basin, where hundreds of hydropower dams are expected to have synergic effects on river dwelling communities and ecosystems (*1*). Greenhouse gas (GHG) emissions represent a critical question in the debate about the benefits versus socioenvironmental costs of hydropower expansion in Amazonia (*2*). Projections of net methane (CH_4) and carbon dioxide (CO_2) emissions from tropical reservoirs support the idea that some hydroelectric complexes may not offer significant advantages to thermal power plants in terms of GHG emissions (*3*). Despite the ongoing debate regarding the intensity of carbon emissions linked to hydropower generation, hydropower plants became an important destination for certified emission reduction credits issued by the Kyoto Protocol's Clean Development Mechanism (*4*). Considering that different types of hydropower projects may have distinctly different impacts on the GHG budget, it is critical to understand the behavior of carbon fluxes in multiple reservoir settings and conditions. Nevertheless, most of the information available so far does not consider prereservoir emissions nor the magnitude of GHG fluxes right after the reservoir filling.

The Belo Monte complex in the Xingu River (Fig. 1) is now the largest hydropower plant in Amazonia. It has one of the largest installed capacities for electricity generation in the world (11,233 MW) and was built as a run-of-the-river (ROR) plant (*5*). ROR hydropower plants operate by obstructing the main river course while diverting a substantial part of the river flow through a secondary channel. Although they may vary in design, the operation of ROR plants is based on the natural river flow and requires smaller reservoirs than storage-based projects. Consequently, such projects have been regarded as a more sustainable alternative (*6*), but the impacts of structures with the scale of the Belo Monte reservoirs are yet to be understood.

Considering its type, location, and recent installation, the Belo Monte reservoirs constitutes a crucial case study to broaden the current knowledge about the GHG emissions from new hydropower plants in the Amazonian scenario. In this study, we investigated how modern state-of-the-art ROR hydropower design and implementation influenced GHG emissions. We also correlated both total emissions per area and emission per energy production capacity with other Amazonian reservoirs to support strategic decisions on future damming projects. To accomplish that, CH_4 and CO_2 fluxes in the Belo Monte area were measured during the high- and low-water seasons of the first 2 years after the filling of the reservoirs and compared to preexisting natural GHG emissions in the affected region.

RESULTS

Physical and chemical characteristics of the reservoirs

Water dissolved oxygen, wind speed, pH, and air and surface water temperature at the sampling sites were relatively similar during pre- and postflooding conditions. Surface water temperatures (30.2° ± 1.2°C) and air temperatures (30.4° ± 2.2°C) had relatively low variation during our sampling campaigns, with slightly higher values during the low-water season. Average pH values (6.8 ± 0.4) were seasonally and spatially stable. Wind speeds varied from 1.9 ± 0.2 over flooded soils to 3.2 ± 0.3 m s^{-1} on the river channel. Dissolved oxygen was also lower in flooded areas (6.2 ± 0.5 mg $liter^{-1}$) than in the main channel (6.9 ± 0.1 mg $liter^{-1}$).

[1]Institute of Geosciences, University of São Paulo, São Paulo, SP, Brazil. [2]Department of Thematic Studies – Environmental Change, Linköping University, Linköping, Sweden. [3]Faculty of Biological Sciences, Federal University of Pará, Altamira, PA, Brazil. [4]Center of Nuclear Energy in Agriculture, University of São Paulo, Piracicaba, SP, Brazil. [5]School of Oceanography, University of Washington, Seattle, WA, USA.
*Corresponding author. Email: dailson.bertassoli@usp.br
†Present address: School of Arts, Sciences and Humanities, University of São Paulo, São Paulo, SP, Brazil.

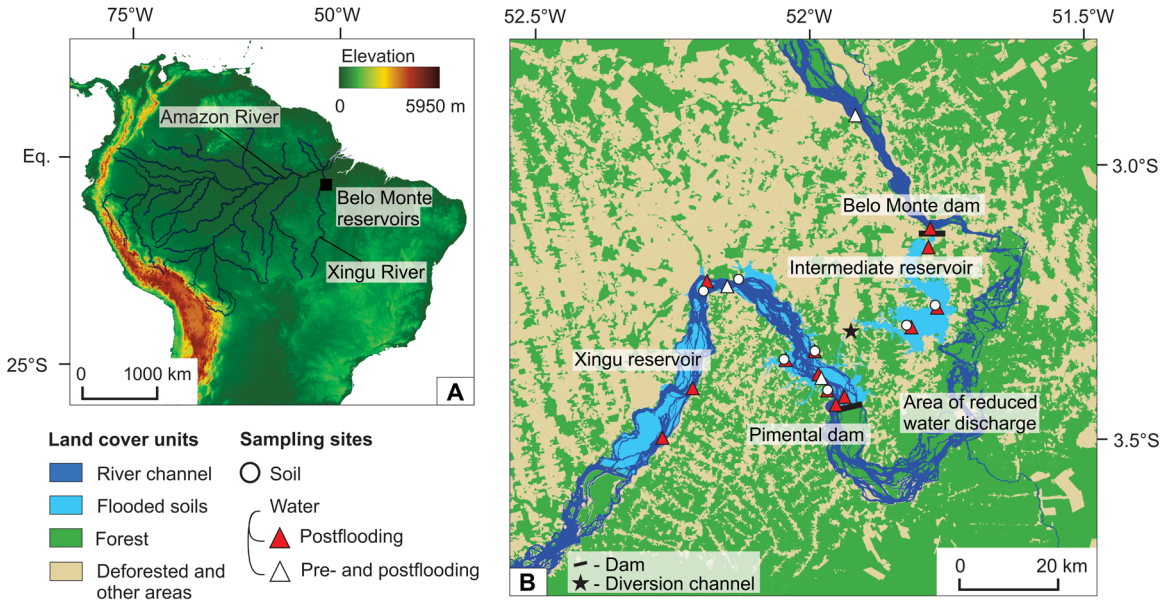

Fig. 1. Study area and sampling location. (**A**) The Amazon River Basin and location of the Belo Monte hydropower complex [Shuttle Radar Topography Mission (*35*)]. (**B**) Land-use maps (*36*) depicting flooded areas, the original river channel, and sampling sites to assess pre- and postimpoundment emissions. Coordinates are presented in tables S2 and S3.

Preflooding emissions in the Belo Monte reservoirs area

Estimated preflooding emissions from the Xingu River channel and from soils later flooded by the Belo Monte reservoirs area are presented in Fig. 2 and table S1. Fluxes of CO_2 (FCO_2) and CH_4 (FCH_4) from soils to the atmosphere are higher during the high-water season (Fig. 2). Notably, we did not observe significant differences between emissions from pasture and forest-covered soils (U = 158, P > 0.05, n = 38). Preimpoundment FCH_4 and partial pressures of CH_4 (pCH_4; the partial pressure equivalent of the water concentration according to Henry's law) in the Xingu River channel were higher during the low-water season (Fig. 2). FCO_2, on the other hand, reached maximum values during the high-water season (Fig. 2). Ebullitive fluxes were identified in the river channel in four of the nine measurements during the preimpoundment campaign. Still, about 70% of the total FCH_4 was related to diffusive fluxes (average of contribution per sample). Preflooding emissions of CH_4 were higher in the river channel than in soils, while the opposite was observed for CO_2. FCO_2 from soils accounted for roughly 80% of the combined gross emissions, considering equivalent CO_2 emissions estimates (FCO_2eq) (see Materials and Methods).

Postflooding and net emissions from the Belo Monte reservoirs

Ebullitive fluxes were identified in about 75% of the sampling sites, without significant seasonal changes of average emissions (U = 314.5, P > 0.05, n = 34). pCH_4 and FCH_4 were also seasonally stable [$U(FCH_4)$ = 347.5, $U(pCH_4)$ = 353, P > 0.05, n = 34], but with higher values measured over flooded soils (Fig. 2). FCH_4 and pCH_4 from areas downstream of the reservoirs, close to the Pimental and Belo Monte dams, were markedly lower than measurements taken from the reservoirs (upstream of the dams) during the low-water season (table S1). During the high-water season, on the other hand, downstream FCH_4 and pCH_4 were relatively similar to channel values upstream of the dam. However, some uncertainty still remains from the hydrodynamic changes in the area of reduced water discharge downstream of the Pimental dam (Fig. 1). FCO_2 values presented in Fig. 2 and tables S1 and S2 represent the average results obtained from previous literature (*7*). The marked seasonal contrast in FCO_2 from flooded soils is mostly related to exceptionally high emissions from the intermediate reservoir during the low-water season (n = 3; 409.2 to 1037.4 mmol CO_2 m^{-2} day^{-1}). With exception of these results, FCO_2 from flooded soils also show seasonal stability (U = 29, P > 0.05, n = 16). Nevertheless, FCO_2 can vary substantially at a single site, as indicated in fig. S1. In the river channel, except for increased FCO_2 during the low-water season, CH_4 and CO_2 emissions were in the same range as observed during preflooding campaigns (Fig. 2). Flooded areas, on the other hand, presented FCH_4 two orders of magnitude higher than before impoundment. This increase roughly tripled the FCO_2eq fluxes (table S1).

By extrapolating the obtained flux to the entire area and considering seasonal heterogeneities, it was possible to estimate the average FCH_4 and FCO_2 at the Belo Monte reservoirs during the first 2 years after the impoundment. FCH_4 ranged from 6.5 to 17.7 mmol CH_4 m^{-2} day^{-1} [confidence interval (CI) = 95%] and FCO_2 from 83.1 to 202.3 mmol CO_2 m^{-2} day^{-1} [CI = 95% (*7*)]. The obtained values correspond to about 0.02 to 0.05 Tg (Teragram) CH_4 $year^{-1}$ and 0.33 to 1.12 Tg CO_2 $year^{-1}$, which are equivalent to emissions of 1.8 to 3.2 Tg CO_2eq $year^{-1}$ (Table 1). By subtracting the spatially averaged preflooding emissions and accounting for changes in vegetation and downstream fluxes, we estimate an average net emission (ΔF) of 0.6 to 2.2 Tg CO_2eq $year^{-1}$. Considering the obtained emissions (FCO_2eq and ΔF) and the declared firm capacity of 4.571 MW (*8*), the estimated gross and net emission factors per total energy production capacity of the Belo Monte reservoirs were from 45 to 79 and 15 to 55 kg CO_2eq MWh^{-1}, respectively.

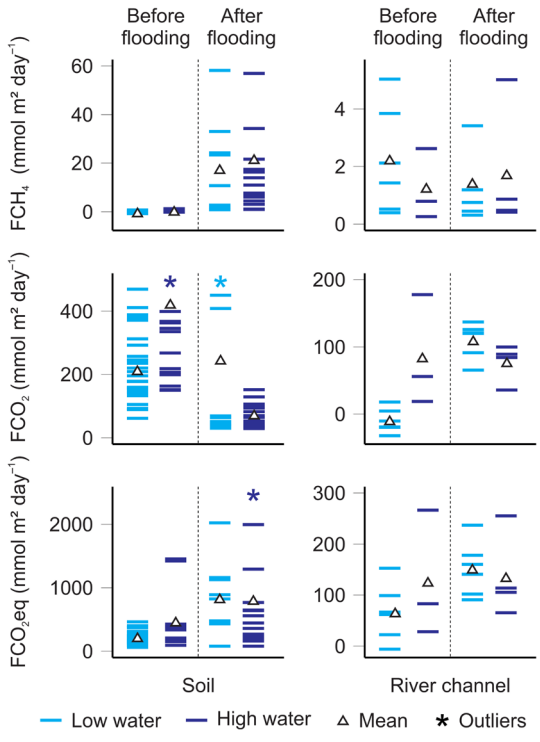

Fig. 2. Fluxes of CH_4 and CO_2 in the reservoir area. Plots of FCH_4, FCO_2 (*7*), and FCO_2eq. Four outliers are not presented in the graphs to maintain a proper scale. Averages, SEs, and additional data are presented in table S2.

DISCUSSION

Our results show that the establishment of the Belo Monte hydropower plant significantly affected local FCH_4 and FCO_2. FCO_2eq from flooded soils nearly doubled in relation to measurements on preflooded conditions. This increase was attributed to the higher FCH_4 from flooded soils due to the degradation of residual organic matter under anoxic conditions (*9*). In contrast, seasonally averaged FCH_4 in the flooded channel and downstream of the dam were not remarkably different from emissions in the unaltered river channel. This reinforces the importance of spatial variations in estimations of CH_4 emissions in newly flooded tropical reservoirs. Part of the contrasting results seen in the literature regarding the GHG footprint of hydroelectric reservoirs is probably related to the fact that several estimates are based on a low number of sampling sites that could diminish the disproportionate contribution of hotspots (i.e., drawdown areas) and periods of intense ebullition (i.e., caused by fluctuating water levels) (*10*).

Ebullitive fluxes are possibly the major source of uncertainties for gross GHG emissions estimates in the Belo Monte reservoirs due to their spatially uneven distribution and episodic nature. Previous studies have shown that the slowdown of river water, which happens in all types of reservoirs, induces sedimentation of organic particles leading to increased organic matter available for degradation and higher ebullition (*11*). In our study, higher ebullition was observed in shallow flooded areas and reinforces the importance of measurements in marginal flooded zones, which can represent up to 45% of the total system emission (*12*, *13*). This is particularly important, as water level fluctuations due to operational requirements could also influence CH_4 ebullition (*14*). Nevertheless, as FCH_4 was relatively constant over time, changes in hydrostatic pressures due to seasonal water level changes may not be the main factor of variability in the studied reservoirs.

Our calculations suggest that ebullition contributed to about half of FCH_4, which is in agreement with previous estimates for other reservoirs and natural lakes [about 50% (*10*, *15*)]. Total ebullition from the flooded river channel only accounted for about 20% of total emissions and could, if used for extrapolation, lead to a substantial underestimation of FCH_4.

Values of pCO_2 and pCH_4 from the water column close to the intake of the turbines are low and suggest that degassing in the outflow of the turbines may not be as notable as in traditional reservoirs. These results are consistent with the fact that the water intakes of the Belo Monte and Pimental dams are in relatively shallow positions (15- to 20-m water depth). However, FCH_4 and FCO_2 measurements taken 0.3, 1.5, and 30 km downstream of the turbines outflow differ from preflooding emissions of the Xingu River channel and suggest that fluxes downstream of the dams changed after the impoundment (table S1).

The possibility and potential impact of carbon burial in reservoirs have been debated. Although reservoirs may increase carbon burial efficiency, this process is still poorly understood and difficult to quantify (*16*). In this study, aggregate emissions estimations (Table 1) do not consider carbon burial in the reservoirs as an offset to GHG fluxes because most of the particulate organic matter would already settle further downstream within the Xingu Ria, a broad "lake-like" channel with calm waters that traps most of the Xingu suspended sediments (*17*).

Overall, our results indicate that postflooding gross emissions in the Belo Monte reservoirs are two- to threefold higher than emissions before the damming (Table 1). Notably, ΔF values obtained in this study (0.6 to 2.2 Tg CO_2eq $year^{-1}$) are in the range of previous estimates for the first years of operation of the Belo Monte hydropower complex using a predictive modeling approach (*3*). In this regard, the Belo Monte reservoirs presented the highest energy density per flooded area and lowest predicted emission factor (kg CO_2eq MWh^{-1}) among the 18 new reservoirs (recently built, under construction, or planned) assessed by such models (*3*). GHG emissions from several of Amazonian reservoirs are comparable to those of fossil fuel–based plants (Fig. 3) (*3*).

Age, latitude, air temperature, and chlorophyll α concentrations have been suggested as suitable predictors for FCH_4 and FCO_2 from reservoirs (*10*, *18*). In Fig. 4, we compare our results to a dataset of tropical and extratropical reservoirs of different ages (*10*). The pronounced differences in reservoir geometry and residence time in the studied ROR reservoirs do not seem to influence per-area fluxes substantially. Although previous literature only found a weak correlation between CH_4 emissions and latitude ($P = 0.05$, $R^2 = 0.04$) in this dataset (*10*), the distributions of reported total emissions (diffusive + ebullitive) from tropical ($n = 20$) and extratropical ($n = 32$) regions differ significantly ($P < 0.05$; Fig. 4). The same occurs for diffusive fluxes ($n_{tropical} = 15$, $n_{extra} = 91$, $P < 0.05$). The average emissions from the Belo Monte reservoirs were on the higher end of previously published global values and were similar to mean emissions from tropical reservoirs less than 10 years old (Fig. 4), independently of reservoir type (storage or ROR). Despite that, the estimated gross and net emission factors per firm capacity (EFC, kg CO_2eq MWh^{-1}), which were calculated by dividing the estimated emissions by the minimum assured average energy generation, are

Table 1. Overview of net change in CH_4 and CO_2 fluxes from the area affected by the Belo Monte reservoirs. Fluxes are integrated over the full affected area and a full annual cycle accounting for seasonal differences (see Spatiotemporal analysis and upscaling, table S4, and fig. S6 for details). Aggregate fluxes (F_{t1CH4}, F_{t1CO2}, $F_{gross-pre}$, F_{t2CH4}, F_{t2CO2}, and F_{gross} in table S4) do not take into account potential carbon burial (see Spatiotemporal analysis and upscaling for further explanations). Results are expressed as confidence intervals at 95%. n.a., not available.

Flux type and environment	Area	Preflooding emissions			Postflooding emissions		
	km^2	CH_4 ($Gg\ year^{-1}$)	CO_2 ($Tg\ year^{-1}$)	CO_2eq ($Tg\ year^{-1}$)	CH_4 ($Gg\ year^{-1}$)	CO_2 ($Tg\ year^{-1}$)	CO_2eq ($Tg\ year^{-1}$)
Vertical exchange with atmosphere							
River channel	177–259	[1.16; 3.65]	[0.01; 0.30]	[0.08; 0.39]	[0.87; 3.38]	[0.26; 0.41]	[0.31; 0.49]
Soils	240–353	[0.02; 0.34]	[0.98; 1.67]	[0.99; 1.68]	[16.29; 45.22]	[0.33; 1.12]	[1.06; 2.33]
Urban and mining areas	1	n.a.	n.a.	n.a.	–	–	–
Fluxes linked to vegetation							
Forest	45–67	–	[−0.29; −0.18]	[−0.29; −0.18]	0	0	0
Seasonally flooded forest	53–79	[1.83; 5.85]	[−0.34; −0.21]	[−0.25; −0.05]	[0.73; 2.34]	[−0.14; −0.08]	[−0.10; −0.02]
Grasslands and pioneering vegetation	140–210	–	[−0.47; −0.26]	[−0.47; −0.26]	0	0	0
Vertical exchange with sediments							
Potential carbon burial	398–543	–	–	–	–	–	[−0.27; −0.80]
Fluxes from downstream of the dams							
Turbine degassing	–	–	–	–	n.a.	n.a.	n.a.
Fluxes downstream of the dams	233–341, 193–283	[1.51; 4.80]	[0.02; 0.39]	[0.10; 0.50]	[0.68; 1.88]	[0.22; 0.64]	[0.26; 0.67]
Aggregate flux	–	[4.72; 9.19]	[0.30; 1.21]	[0.59; 1.52]	[20.31; 49.36]	[0.91; 1.85]	[1.79; 3.18]

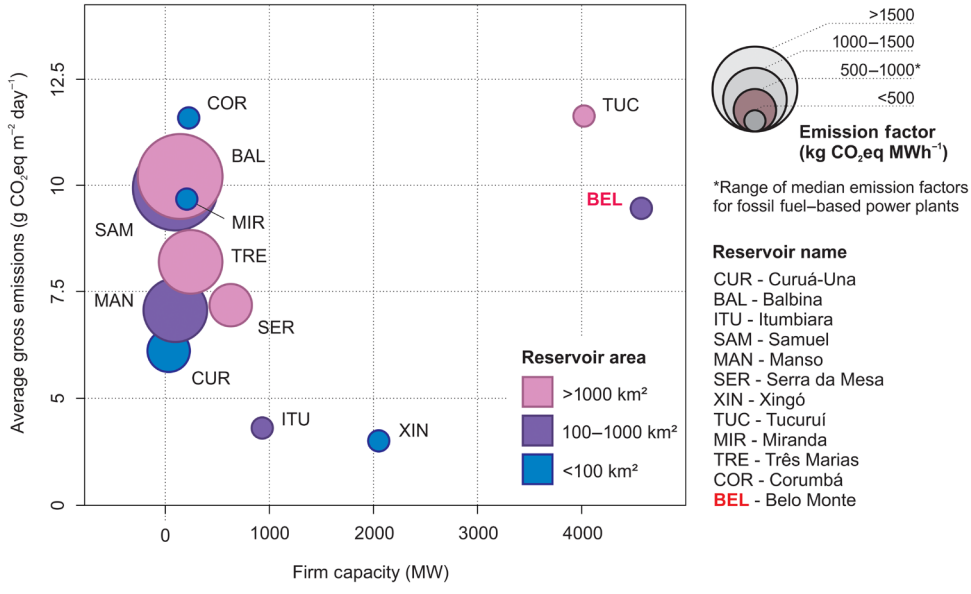

Fig. 3. Mean CO_2eq emissions per area compared to the firm capacity of Brazilian hydroelectric power plants. Life-cycle emission factors of thermal power plants are presented for comparison (*19*). Besides Belo Monte reservoirs (BEL) results from this study, we used emission values [(*10*) and references therein] and firm capacities (*8*) compiled from the literature.

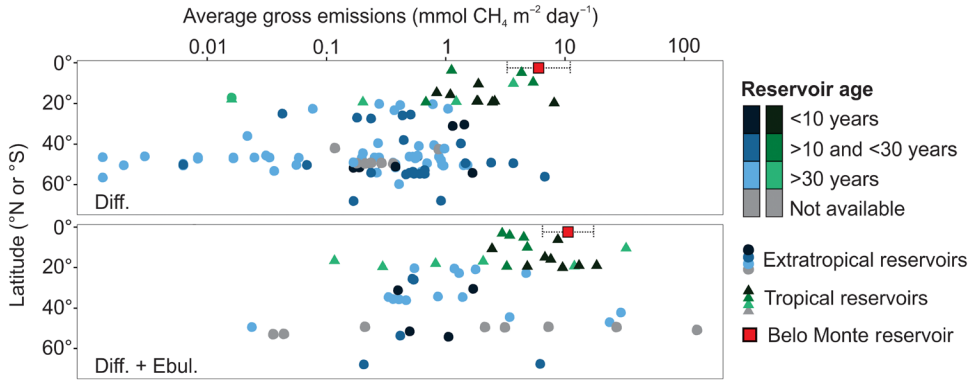

Fig. 4. Average CH_4 emissions per area from hydroelectric reservoirs compared to the Belo Monte reservoirs. Compiled data of average CH_4 emissions per area [(*10*) and references therein] compared to Belo Monte data (this study).

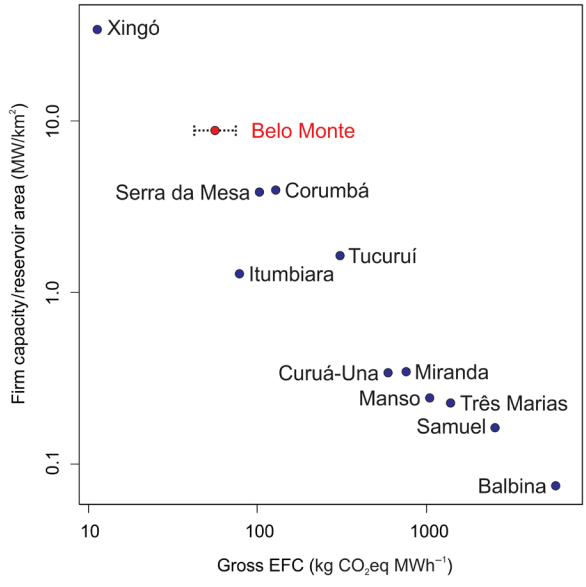

Fig. 5. Scatterplots comparing gross EFC and the ratio of firm energy capacity to reservoir area. Besides Belo Monte reservoirs data (our study), we used emission values compiled from the literature [(*10*) and references therein]. $R^2 = 0.98$, $P < 0.05$. Axes are in log-scale.

lower than other major Brazilian hydropower plants (i.e., Figs. 3 and 5). It is also notable that calculated EFCs are substantially higher than the values presented in life cycle estimates for ROR power plants in previous literature (*19*, *20*). However, our data only account for direct reservoir emissions and, therefore, should not be interpreted as a complete life cycle assessment.

Projections show a sharp decline in the Belo Monte's firm capacity for the next decades (up to ~38%) due to the current trends of climate change and deforestation (*21*). As such, life cycle assessments should account for downward adjustments in energy generation potential that could severely affect the calculated gross and net EFC. Nevertheless, given the strong dependence of EFC on power density (firm capacity per flooded area), our results indicate that when it comes to GHG emissions, efforts should be focused on reducing the flooded area, which tends to be minimized in ROR hydropower plants. Regardless of the average emissions per area, reported Brazilian hydroelectric reservoirs with power density below 0.5 MW km^{-2} exhibited gross EFC comparable or higher than those of thermal power plants (Figs. 3 and 5). The global warming potential (GWP) of the Belo Monte reservoirs during the first years of operation represents up to ~10% of natural gas plants (422 to 548 kg CO_2eq MWh^{-1}) and is comparable to those related to nuclear power plants (8 to 45 kg CO_2eq MWh^{-1}) or other renewable sources such as photovoltaic (29 to 80 kg CO_2eq MWh^{-1}) and wind power plants (8 to 20 kg CO_2eq MWh^{-1}) [25th to 75th percentiles (*19*)].

The remarkable social and environmental costs of reservoirs are key elements for the evaluation of the viability of hydropower projects. Predictive models to estimate the GHG emissions of future reservoirs are a powerful tool in environmental studies and indispensable to move toward a more sustainable energy generation in terms of GHG. Specifically for the Amazon River Basin, recent efforts represent a great advance toward the development of strategies to achieve sustainable energy goals (*3*, *22*). In such light, our results may also be used as a validation of previous models (*3*) and provide a new perspective on strategic planning. Given the intensity of carbon emissions also for state-of-the-art ROR reservoirs such as Belo Monte, in combination with all other social and environmental costs of Amazonian reservoirs, we urge decision-makers to consider alternatives for energy generation that avoid the impoundment of large rivers and creation of new flooded areas in this region.

MATERIALS AND METHODS

Study area

The Xingu River is the second largest tributary in the eastern Amazon River Basin (Fig. 1). It drains about 500,000 km^2 of an area with regional climate defined by a rainy/high-water season from December to May and dry/low-water season from June to November (fig. S2) (*23*). The Xingu River has a relatively low suspended sediment load (< 20 mg $liter^{-1}$), and its water discharge varies from about 1000 to 20,000 m^{-3} s^{-1} (*23*).

Previous assessments of GHG emissions in Amazonian rivers showed that rivers with relatively low organic and suspended sediment loads (clearwater rivers) have the highest potential for CH_4 emissions (*24*). Accordingly, the Xingu River was previously observed to have the highest emissions per area, with total CH_4 fluxes being 1- to 100-fold larger than fluxes from other Amazonian rivers like the Madeira, Negro, and Solimões. The Xingu River also had

the lowest CH_4 oxidation rates (equivalent to 28 to 67% of the diffusive flux of CH_4) and the highest ebullition fluxes compared to the other large Amazonian rivers (equivalent to 50% of the total CH_4 emissions) (*24*, *25*).

The Belo Monte hydropower complex was installed in the lower reach of the Xingu River, over a system of multiple rocky channels known as Volta Grande do Xingu ("Xingu Great Bend", Fig. 1). This stretch presents an exceptionally diverse and endemic fish fauna (*26*) and is full of rapids and waterfalls with unique and high scenic value. Despite the intense controversy regarding the energy benefits in terms of the potential socioenvironmental impacts of this project (*2*), the Belo Monte reservoirs were filled during the high-water season of 2016.

The Belo Monte reservoirs flooded an area of about 516 km^2 (*5*). It covers a stretch of approximately 80 km of the Xingu River ("Xingu reservoir") and a flooded valley that is also known as the "intermediate reservoir." Both areas are connected through a diversion channel (Fig. 1). According to the environmental impact studies presented to the Brazilian government (*5*), nearly 122 km^2 (23.7%) of the flooded area was previously covered by rainforest; 175 km^2 (33.9%) by pasturelands, plantations, and secondary and pioneering vegetation; and 1 km^2 (0.2%) by urban and mining areas. Notably, about 114 km^2 of the forest and grasslands were seasonally flooded by the Xingu River before the impoundment.

In the Belo Monte complex, the Pimental dam impounded the Xingu channel to redirect most of the water flux to the intermediate reservoir formed by the Belo Monte dam (Fig. 1). The Belo Monte dam holds more than 95% of the installed capacity (has 18 Francis-type turbines with 611 MW each), while the Pimental dam mainly regulates the water flow in the Xingu reservoir and has a minor installed capacity of 233 MW (*5*). The intakes of both dams are above the hypolimnion, at a depth of about 15 to 20 m. The water stage in the reservoirs is highly variable, and peak energy generation is projected to only occur during periods of maximum water discharge. Since most of the wet season water flux is redirected for hydropower generation at the Belo Monte dam, a stretch of about 100 km between the Pimental and the Belo Monte dams has been subjected to a reduced supply of water (Fig. 1). As such, the multiple bedrock channels, rapids, and waterfalls in this area may face remarkable changes in their hydrologic regimes.

Sampling scheme

Sampling sites were selected considering the heterogeneous hydrodynamic conditions of the reservoirs and the different types of vegetation cover before the flooding. We measured CH_4 fluxes to the atmosphere 67 times along 23 different sites at the Belo Monte reservoirs and downstream of the dams (Fig. 1B). To establish CH_4 emissions from the Xingu River channel before the impoundment, we used data collected by previous assessments (*24*) during the months of May and November of 2012 and performed an additional sampling survey in November and December of 2014. Sampling surveys to measure emissions from the Belo Monte reservoirs after their filling occurred in April of 2016 and in May, September, and October of 2017. Fluxes of CH_4 from terrestrial areas close to the reservoirs were measured in the months of May, September, and October of 2017. In addition, measurements of CO_2 emissions from a single station upstream of the Pimental dam were taken in February, April, and from June to October of 2016. Emissions from soils were used to estimate the background emissions before the filling of the Belo Monte reservoirs.

Floating chambers drifting on running waters were used to measure FCH_4 from aquatic environments following the methods described in previous works (*24*, *27*). Simultaneously, water samples were collected from different depths to determine the pCH_4 using the headspace extraction method (*27*). Depth, water and air temperature, atmospheric pressure, and wind speed were controlled using a sonar sensor and a weather station installed in the boat (Kestrel 5500 weather meter; Nielsen-Kellerman Company, Boothwyn, PA, USA). Physicochemical variables (pH and dissolved oxygen) were measured during three sampling surveys (November of 2012, April of 2016, and May of 2017) using a multiparameter probe (EXO2 multiparameter sonde; YSI Incorporated, Yellow Springs, OH, USA). Physicochemical results presented in this study correspond only to data collected in situ during measurements. Part of the measurements and interpretations presented in this text were also drafted in the doctoral dissertation of the first author (*28*).

Flux measurements from surface waters

CH_4 fluxes from surface waters were obtained using five chambers with volumes of 4 to 12 liters deployed for an average period of 45 min. Chambers were separated approximately 1 m from each other. Characteristics and construction of the chambers followed previously tested setups that showed nonbiased results (*29*, *30*). Air samples were retrieved from floating chambers through an outlet using 60-ml syringes and immediately transferred to preevacuated glass vials (20 ml) sealed with 10-mm-thick butyl rubber stoppers.

Gas concentrations were measured in gas chromatographs (Thermo Fisher Scientific TRACE 1310 and Shimadzu GC17A) equipped with an online methanizer coupled to an flame ionization detector (FID) and by cavity ring-down spectroscopy using a Picarro G2201-i device. Readings from all analyzers were cross-calibrated according to a standard calibration curve.

Total FCH_4 and the relative contribution from diffusive and ebullitive components were calculated according to (*24*) and (*15*, *27*). Diffusive fluxes are described by the equation

$$F = k \cdot (C_w - C_{fc}) \quad (1)$$

where F is flux, k is the gas transfer velocity, C_w is the measured concentration of CH_4 in the water, and C_{fc} is the CH_4 concentration in the water given equilibrium with pCH_4 inside the floating chamber. To obtain the instantaneous flux rate and avoid underestimations linked to the progressive increase of CH_4 concentration inside the floating chamber, we calculated diffusive fluxes through Eq. 1 after solving for k using the following equation

$$k = \left(\frac{dP}{dt}\right) \cdot \frac{V(P_w - P_0)}{K_h \cdot R \cdot T \cdot A} \quad (2)$$

Where dP/dt describes the accumulation of CH_4 inside the chamber (slope of CH_4 accumulation over time), V is the chamber volume, P_w is the pCH_4 inside the chamber at equilibrium with the measured concentration of CH_4 in the water and derives from C_w values obtained through headspace measurements, P_0 is the partial pressure of CH_4 in the atmosphere ($t = 0$), K_h is the Henry's law constant for CH_4, R is the gas constant, T is temperature, and A is the surface area of the chamber.

We used the variation of the apparent temperature-normalized gas transfer velocities (k_{600}) to detect chambers that were affected by

ebullition (*15*). As chambers that received only diffusive fluxes would present similar and lower flux rates, we considered the fluxes of chambers with minimum k_{600} values as the purely diffusive component. The k_{600} of individual chambers were divided by the minimum k_{600} (k_{600min}) of each sampling site, and chambers with ratios above 2 were considered to be significantly affected by ebullitive fluxes. The threshold value (>2) was chosen on the basis of the inflection in the frequency distribution of the k_{600}/k_{600min} ratio (fig. S3). Threshold values around 2 were also found in (*15*).

The diffusive component of chambers with k_{600}/k_{600min} above 2 was estimated using the averaged k_{600} from chambers of the same sampling site and time that only received diffusive flux. The remaining amount, estimated by simple linear regression, was attributed to ebullition. For estimations of total average fluxes, we summed the average ebullition to the average diffusive flux estimated using the k_{600}.

Preimpoundment fluxes of CO_2 (FCO_2) from the Xingu River channel were measured using a similar floating chamber as for the CH_4 measurements (7.7 liters, covered with reflexive material) coupled to an infrared gas analyzer (LI-COR Li820). Changes in CO_2 concentration inside the chamber were measured after recirculating air through the analyzer using a micropump with constant airflow (150 ml min^{-1}). The chamber was deployed from a drifting boat for about 5 min during measurements. Three measurements were carried out for each location. This same protocol was used for monthly postflooding FCO_2 estimates in 2016. These additional measurements were carried out at a single site to verify fluctuations in FCO_2 along the year. To reinforce our evaluation, we also did preflooding measurements during the low-water season of 2014 using CO_2 loggers (*31*) inside two floating chambers used for the CH_4 flux analyses. These chambers were deployed from a drifting boat for about 30 min using a logging frequency of 30 s. Measurements for both methods were discarded when the R^2 of the linear relation of pCO_2 inside the chamber over time was lower than 0.9. The FCO_2 from the water surface was then calculated using the following equation

$$F = \left(\frac{dP}{dt}\right) \cdot \frac{V}{R \cdot T \cdot A} \quad (3)$$

where F is the flux, dP/dt describes the accumulation of gas inside the chamber (slope of CH_4 accumulation over time), V is the chamber volume, R is the gas constant, T is temperature, and A is the surface area of the chamber.

Estimations of CH_4 and CO_2 fluxes from soils

We measured CH_4 and CO_2 fluxes from soils of islands and marginal areas of the Xingu River to refine estimates of GHG emissions from the region affected by the Belo Monte reservoirs before flooding. Sampling sites were distributed over areas with different characteristics and vegetation cover (forest and nonforested areas). Measurements occurred during both low-water (n = 8) and high-water seasons (n = 7). Four of the sampling sites were covered by upland or flooding forest and the others by pasture. Given that one site was seasonally submerged, fluxes were measured using static chambers and counted as soil estimations during the low-water season (GEX-65, table S3) and as flooded area estimations during the high-water season (GEX-14, table S2).

Measurements were made using static chambers with 10.6 liters (n = 3 in the low-water season and n = 4 in the high-water season) equipped with a Teflon tube for sampling. The chambers were composed of a PVC ring and a cap that could be separated. The PVC rings were inserted in the soil at depths ranging from 5 to 10 mm and capped after approximately 3 min. After capping, gas samples were retrieved using a 60-ml syringe every 10 min for a period of 30 min and transferred to evacuated vials. Gas concentration measurements followed the methods previously described in Flux measurements from surface waters. Measurements for both gases were discarded when the R^2 of concentration over time was lower than 0.9, except when variations were lower than 0.1 ppm (fluxes were negligible). Fluxes from soils were estimated using Eq. 3.

Spatiotemporal analysis and upscaling

The spatiotemporal variability of gross CH_4 and CO_2 fluxes in the Belo Monte reservoirs area was assessed by comparing (i) gross emissions before and after the impoundment and flooding, (ii) seasonal variations in emissions of different areas, and (iii) differences between emissions from the flooded river channel and from marginal areas that were inundated by the Belo Monte reservoirs (flooded soils). Data from previous literature were used to account for different parameters affecting gross and net emissions estimates (more information is available at table S4). FCH_4 values were converted to equivalent CO_2 emissions (FCO_2eq) using the 100-year GWP [= 34; (*32*)].

Pre- and postflooding emissions of the Belo Monte reservoirs area correspond to mean fluxes from soil and water surfaces calculated after considering seasonal (low-water and high-water) and spatial (soil and channel areas) heterogeneities. The dimensions of the downstream reaches before and after the impoundment (1984–2018) were obtained from maps provided by (*33*). Areas of other locations were obtained from the environmental impact study from (*5*). Since empirical data regarding the uncertainty of these measurements are lacking, values were sampled from a theoretical uniform distribution. Distribution support was defined assuming deviations from the mean of 10 and 20% for seasonal duration and area, respectively. We also applied a reduction factor of 50 ± 10% in the proportion of the flooded area that is subject to seasonal variation [about 30%, estimated from (*33*)] to account for changes in the dimensions of the reservoirs. As such, measurements done in the low- and high-water periods were extrapolated for about 6 months each. More details are presented in table S4.

The Monte Carlo approach used to estimate mean annual emissions and their corresponding uncertainties depends on the calculation of the probability density function for each group of measurements. Sets of emission data grouped by sampling season and location were compared to different theoretical distributions [fitdistrplus package (*34*)]. Gamma and Weibull distributions were assigned as best representatives for data from flooded soil and channel areas, respectively (figs. S4 and S5). Artificial datasets (n = 10,000) on the basis of the fitted distributions were used in the Monte Carlo estimation. During each of the 10,000 iterations, we computed the arithmetic mean of emission values that were randomly resampled (with replacement) from the artificial datasets. Averages of each group were then extrapolated to their corresponding area and seasonal duration, summed, and added to the database of results. CIs (= 95%) were then calculated from the distribution of the totals stored in the database. A simplified scheme of the upscaling method is given in fig. S6 and calculations are detailed in table S4.

Net emissions (ΔF) were calculated after considering pre- and postflooding gross CO_2eq emissions from vegetation, soil, and water surfaces in the Belo Monte area (table S4). We estimated carbon

burial by reconstructing an artificial dataset (n = 10,000) on the basis of the fitted log-normal distribution of carbon uptake data for the Xingu Ria presented in (*17*). Resampled carbon uptake values were then extrapolated to the entire reservoirs area. The EFC (kg CO_2eq MWh^{-1}) of the Belo Monte hydropower plant was calculated after dividing gross and net emissions by the minimum assured average energy generation of the system [4571 MW; table S4 and (*8*)].

Statistical analyses

Mann-Whitney U tests (two-sided) were used for comparisons between fluxes due to the non-normal distribution of the obtained data. All statistical analyses were performed using 0.05 as a critical α for significance.

SUPPLEMENTARY MATERIALS

Supplementary material for this article is available at http://advances.sciencemag.org/cgi/content/full/7/26/eabe1470/DC1

REFERENCES AND NOTES

1. B. R. Forsberg, J. M. Melack, T. Dunne, R. B. Barthem, M. Goulding, R. C. Paiva, M. V. Sorribas, U. L. Silva Jr., S. Weisser, The potential impact of new Andean dams on Amazon fluvial ecosystems. *PLOS ONE* **12**, e0182254 (2017).
2. E. F. Moran, M. C. Lopez, N. Moore, N. Müller, D. W. Hyndman, Sustainable hydropower in the 21st century. *Proc. Natl. Acad. Sci. U.S.A.* **115**, 11891–11898 (2018).
3. F. A. M. de Faria, P. Jaramillo, H. O. Sawakuchi, J. E. Richey, N. Barros, Estimating greenhouse gas emissions from future Amazonian hydroelectric reservoirs. *Environ. Res. Lett.* **10**, 124019 (2015).
4. P. M. Fearnside, Carbon credit for hydroelectric dams as a source of greenhouse-gas emissions: The example of Brazil's Teles Pires Dam. *Mitig. Adapt. Strat. Glob. Chang.* **18**, 691–699 (2013).
5. Eletrobrás, Aproveitamento Hidrelétrico Belo Monte: Estudo de Impacto Ambiental (Rio de Janeiro), 36 v. (2009).
6. D. Kumar, S. S. Katoch, Sustainability assessment and ranking of run of the river (RoR) hydropower projects using analytical hierarchy process (AHP): A study from Western Himalayan region of India. *J. Mountain Sci.* **12**, 1315–1333 (2015).
7. K. R. de Araújo, H. Sawakuchi, D. J. Bertassoli Jr., A. O. Sawakuchi, K. D. da Silva, T. B. Vieira, N. D. Ward, T. S. Pereira, Carbon dioxide (CO_2) concentrations and emission in the newly constructed Belo Monte hydropower complex in the Xingu River, Amazonia. *Biogeosciences* **16**, 3527–3542 (2019).
8. EPE, Revisão Ordinária de Garantia Física de Energia das Usinas Hidrelétricas—UHEs Despachadas Centralizadamente no Sistema Interligado Nacional—SIN (Empresa de Pesquisa Energética, Brasília, 2017), pp. 104.
9. V. Peters, R. Conrad, Sequential reduction processes and initiation of CH_4 production upon flooding of Oxic upland soils. *Soil Biol. Biochem.* **28**, 371–382 (1996).
10. B. R. Deemer, J. A. Harrison, S. Li, J. J. Beaulieu, T. DelSontro, N. Barros, J. F. Bezerra-Neto, S. M. Powers, M. A. Dos Santos, J. A. Vonk, Greenhouse gas emissions from reservoir water surfaces: A new global synthesis. *Bioscience* **66**, 949–964 (2016).
11. T. DelSontro, M. J. Kunz, T. Kempter, A. Wüest, B. Wehrli, D. B. Senn, Spatial heterogeneity of methane ebullition in a large tropical reservoir. *Environ. Sci. Technol.* **45**, 9866–9873 (2011).
12. C. Deshmukh, D. Serça, C. Delon, R. Tardif, M. Demarty, C. Jarnot, Y. Meyerfeld, V. Chanudet, P. Guédant, W. Rode, Physical controls on CH_4 emissions from a newly flooded subtropical freshwater hydroelectric reservoir: Nam Theun 2. *Biogeosciences* **11**, 4251–4269 (2014).
13. S. Natchimuthu, I. Sundgren, M. Gålfalk, L. Klemedtsson, P. Crill, Å. Danielsson, D. Bastviken, Spatiotemporal variability of lake CH_4 fluxes and its influence on annual whole lake emission estimates. *Limnol. Oceanogr.* **61**, S13–S26 (2016).
14. J. A. Harrison, B. R. Deemer, M. K. Birchfield, M. T. O'Malley, Reservoir water-level drawdowns accelerate and amplify methane emission. *Environ. Sci. Technol.* **51**, 1267–1277 (2017).
15. D. Bastviken, J. Cole, M. Pace, L. Tranvik, Methane emissions from lakes: Dependence of lake characteristics, two regional assessments, and a global estimate. *Global Biogeochem. Cycles* **18**, GB4009 (2004).
16. Y. T. Prairie, J. Alm, J. Beaulieu, N. Barros, T. Battin, J. Cole, P. del Giorgio, T. DelSontro, F. Guérin, A. Harby, J. Harrison, S. Mercier-Blais, D. Serça, S. Sobek, D. Vachon, Greenhouse gas emissions from freshwater reservoirs: What does the atmosphere see? *Ecosystems* **21**, 1058–1071 (2018).
17. D. J. Bertassoli Jr., A. O. Sawakuchi, H. O. Sawakuchi, F. N. Pupim, G. A. Hartmann, M. M. McGlue, C. M. Chiessi, M. Zabel, E. Schefuß, T. S. Pereira, The fate of carbon in sediments of the Xingu and Tapajós clearwater rivers, Eastern Amazon. *Front. Mar. Sci.* **4**, 44 (2017).
18. N. Barros, J. J. Cole, L. J. Tranvik, Y. T. Prairie, D. Bastviken, V. L. Huszar, P. del Giorgio, F. Roland, Carbon emission from hydroelectric reservoirs linked to reservoir age and latitude. *Nat. Geosci.* **4**, 593–596 (2011).
19. W. Moomaw, P. Burgherr, G. Heath, M. Lenzen, J. Nyboer, A. Verbruggen, Annex II: Methodology in *IPCC Special Report on Renewable Energy Sources and Climate Change Mitigation*, R. P.-M. O. Edenhofer, Y. Sokona, K. Seyboth, P. Matschoss, S. Kadner, T. Zwickel, P. Eickemeier, G. Hansen, S. Schlömer, C. von Stechow, eds. (Cambridge Univ. Press, 2011).
20. H. L. Raadal, L. Gagnon, I. S. Modahl, O. J. Hanssen, Life cycle greenhouse gas (GHG) emissions from the generation of wind and hydro power. *Renew. Sustain. Energy Rev.* **15**, 3417–3422 (2011).
21. C. M. Stickler, M. T. Coe, M. H. Costa, D. C. Nepstad, D. G. McGrath, L. C. Dias, H. O. Rodrigues, B. S. Soares-Filho, Dependence of hydropower energy generation on forests in the Amazon Basin at local and regional scales. *Proc. Natl. Acad. Sci.* **110**, 9601–9606 (2013).
22. R. M. Almeida, Q. Shi, J. M. Gomes-Selman, X. Wu, Y. Xue, H. Angarita, N. Barros, B. R. Forsberg, R. García-Villacorta, S. K. Hamilton, J. M. Melack, M. Montoya, G. Perez, S. A. Sethi, C. P. Gomes, A. S. Flecker, Reducing greenhouse gas emissions of Amazon hydropower with strategic dam planning. *Nat. Commun.* **10**, 4281 (2019).
23. ANA. HidroWeb — Sistema de Informações Hidrológicas (2019); http://snirh.gov.br/hidroweb/[accessed 12 June 2019).
24. H. O. Sawakuchi, D. Bastviken, A. O. Sawakuchi, A. V. Krusche, M. V. Ballester, J. E. Richey, Methane emissions from Amazonian Rivers and their contribution to the global methane budget. *Glob. Chang. Biol.* **20**, 2829–2840 (2014).
25. H. O. Sawakuchi, D. Bastviken, A. O. Sawakuchi, N. D. Ward, C. D. Borges, S. M. Tsai, J. E. Richey, M. V. R. Ballester, A. V. Krusche, Oxidative mitigation of aquatic methane emissions in large Amazonian rivers. *Glob. Chang. Biol.* **22**, 1075–1085 (2016).
26. M. Camargo, T. Giarrizzo, V. Isaac, Review of the geographic distribution of fish fauna of the Xingu river basin, Brazil. *Ecotropica* **10**, 123–147 (2005).
27. D. Bastviken, A. L. Santoro, H. Marotta, L. Q. Pinho, D. F. Calheiros, P. Crill, A. Enrich-Prast, Methane emissions from Pantanal, South America, during the low water season: toward more comprehensive sampling. *Environ. Sci. Technol.* **44**, 5450–5455 (2010).
28. D. J. Bertassoli Jr., Doctoral Dissertation, University of São Paulo (2019).
29. J. J. Cole, D. L. Bade, D. Bastviken, M. L. Pace, M. Van de Bogert, Multiple approaches to estimating air-water gas exchange in small lakes. *Limnol. Oceanogr. Methods* **8**, 285–293 (2010).
30. A. Lorke, P. Bodmer, C. Noss, Z. Alshboul, M. Koschorreck, C. Somlai-Haase, D. Bastviken, S. Flury, D. McGinnis, A. Maeck, D. Müller, K. Premke, Technical note: Drifting vs. anchored flux chambers for measuring greenhouse gas emissions from running waters. *Biogeosciences* **12**, 7013–7024 (2015).
31. D. Bastviken, I. Sundgren, S. Natchimuthu, H. Reyier, M. Gålfalk, Technical Note: Cost-efficient approaches to measure carbon dioxide (CO_2) fluxes and concentrations in terrestrial and aquatic environments using mini loggers. *Biogeosciences* **12**, 3849–3859 (2015).
32. Intergovernmental Panel on Climate Change, *Climate Change 2013: The Physical Science Basis. Contribution of Working Group I to the Fifth Assessment Report of the Intergovernmental Panel on Climate Change*, T. F. Stocker, D. Qin, G.-K. Plattner, M. Tignor, S. K. Allen, J. Boschung, A. Nauels, Y. Xia, V. Bex, P.M. Midgley, eds. (Cambridge Univ. Press, 2013), pp. 1535.
33. J.-F. Pekel, A. Cottam, N. Gorelick, A. S. Belward, High-resolution mapping of global surface water and its long-term changes. *Nature* **540**, 418–422 (2016).
34. M. L. Delignette-Muller, C. Dutang, fitdistrplus: An R package for fitting distributions. *J. Stat. Softw.* **64**, 1–34 (2015).
35. T. G. Farr, P. A. Rosen, E. Caro, R. Crippen, R. Duren, S. Hensley, M. Kobrick, M. Paller, E. Rodriguez, L. Roth, D. Seal, S. Shaffer, J. Shimada, J. Umland, M. Werner, M. Oskin, D. Burbank, D. Alsdorf, The shuttle radar topography mission. *Rev. Geophys.* **45**, RG2004 (2007).
36. C. A. de Almeida, A. C. Coutinho, J. C. D. M. Esquerdo, M. Adami, A. Venturieri, C. G. Diniz, N. Dessay, L. Durieux, A. R. Gomes, High spatial resolution land use and land cover mapping of the Brazilian Legal Amazon in 2008 using Landsat-5/TM and MODIS data. *Acta Amazon.* **46**, 291–302 (2016).
37. A. C. da Costa, D. B. Metcalfe, C. E. Doughty, A. A. de Oliveira, G. F. Neto, M. C. da Costa, J. d. A. S. Junior, L. E. Aragão, S. Almeida, D. R. Galbraith, L. M. Rowland, P. Meir, Y. Malhi, Ecosystem respiration and net primary productivity after 8–10 years of experimental through-fall reduction in an eastern Amazon forest. *Plant Ecol. Diver.* **7**, 7–24 (2014).
38. T. R. Feldpausch, M. A. Rondon, E. C. Fernandes, S. J. Riha, E. Wandelli, Carbon and nutrient accumulation in secondary forests regenerating on pastures in central Amazonia. *Ecol. Appl.* **14**, 164–176 (2004).
39. S. R. Pangala, A. Enrich-Prast, L. S. Basso, R. B. Peixoto, D. Bastviken, E. R. Hornibrook, L. V. Gatti, H. Marotta, L. S. B. Calazans, C. M. Sakuragui, W. R. Bastos, O. Malm, E. Gloor,

J. B. Miller, V. Gauci, Large emissions from floodplain trees close the Amazon methane budget. *Nature* **552**, 230–234 (2017).
40. INMET, Banco de dados meterológicos (2020); https://portal.inmet.gov.br/ [accessed 22 June 2019].
41. Intergovernmental Panel on Climate Change, *2006 IPCC Guidelines for National Greenhouse Gas Inventories, Prepared by the National Greenhouse Gas Inventories Programme*, H. S. Eggleston, L. Buendia, K. Miwa, T. Ngara, K. Tanabe, eds. (IGES, Japan, 2006).

Acknowledgments: We are grateful to F. da Silva Loureiro for safely guiding us in the Xingu River and H. Silva, L. Sousa, T. Akabane, and A. Figueiredo for all the help during the field surveys. We also thank A. Montebelo for laboratory assistance. **Funding:** We acknowledge funding through the São Paulo Research Foundation (FAPESP) (grant numbers 2014/21564-2, 2015/09187-1, 2016/11141-2, 2016/02656-9, 2019/24977-0, 2018/15123-4. 2019/24349-9, 2011/14502-2, and 2018/18491-4) and through the National Science Foundation DEB-1754317. A.O.S. is funded by Conselho Nacional de Desenvolvimento Científico e Tecnológico (CNPq grant 304727/2017-2). D.B. was funded by the European Research Council (ERC; grant agreement 725546), the Swedish Research Council VR, and FORMAS. **Author contributions:** D.J.B., H.O.S., J.E.R., D.B., and A.O.S. were responsible for the design of the study and preparation of the manuscript. A.O.S., H.O.S., D.J.B., A.V.K., and T.S.P. organized overall project logistics. Measurements were done by D.J.B., H.O.S., A.O.S., K.R.d.A., M.G.P.d.C., and V.A.T.A. All authors contributed to data interpretation and critically revised the manuscript for final submission. **Competing interests:** The authors declare that they have no competing interests. **Data and materials availability:** All data needed to evaluate the conclusions in the paper are present in the paper and/or the Supplementary Materials. Additional data related to this paper may be requested from the authors.

Submitted 3 August 2020
Accepted 14 May 2021
Published 25 June 2021
10.1126/sciadv.abe1470

Citation: D. J. Bertassoli Jr., H. O. Sawakuchi, K. R. de Araújo, M. G. P. de Camargo, V. A. T. Alem, T. S. Pereira, A. V. Krusche, D. Bastviken, J. E. Richey, A. O. Sawakuchi, How green can Amazon hydropower be? Net carbon emission from the largest hydropower plant in Amazonia. *Sci. Adv.* **7**, eabe1470 (2021).

Science Advances

How green can Amazon hydropower be? Net carbon emission from the largest hydropower plant in Amazonia

Dailson J. Bertassoli, Jr., Henrique O. Sawakuchi, Kleiton R. de Araújo, Marcelo G. P. de Camargo, Victor A. T. Alem, Tatiana S. Pereira, Alex V. Krusche, David Bastviken, Jeffrey E. Richey and André O. Sawakuchi

Sci Adv **7** (26), eabe1470.
DOI: 10.1126/sciadv.abe1470